Article

Tunable Terahertz Metamaterial Using an Electric Split-Ring Resonator with Polarization-Sensitive Characteristic

Tao Xu and Yu-Sheng Lin *

State Key Laboratory of Optoelectronic Materials and Technologies, School of Electronics and Information Technology, Sun Yat-Sen University, Guangzhou 510275, China; xutao8@mail2.sysu.edu.cn

* Correspondence: linyoush@mail.sysu.edu.cn

Abstract: We present a tunable terahertz (THz) metamaterial using an electric split-ring resonator (eSRR), which exhibits polarization-sensitive characteristics. The proposed eSRR is composed of double symmetrical semicircles and two central metal bars. By changing the lengths of two metal bars, the electromagnetic responses can be tuned and switched between dual-band and triple-band resonances in transverse magnetic (TM) mode. Furthermore, by moving the bottom metal bar to change the gap between the two metal bars, the first resonance is stable at 0.39 THz, and the second resonance is gradually blue-shifted from 0.83 to 1.33 THz. The tuning range is 0.50 THz. This means that the free spectrum ranges (FSR) could be broadened by 0.50 THz. This proposed device exhibits a dual-/triple-band switch, tunable filter, tunable FSR and polarization-dependent characteristics. It provides an effective approach to perform tunable polarizer, sensor, switch, filter and other optoelectronics in THz-wave applications.

Keywords: metamaterial; terahertz optics; optical switch; optical filter; tunable resonator

1. Introduction

It is generally accepted that the terahertz (THz) range is the frequency range of 0.1–10 THz. In recent years, THz technology has attracted growing attention with the progress of THz sources and instrumentation [1,2]. THz technology has been widely used in many fields, including but not limited to filtration [3], molecule identification [4], imaging [5,6] and environmental monitoring systems [7] because it has many fascinating electromagnetic characteristics, such as being harmless to the human body and having artificial magnetism and high chemical sensitivity [8–11]. However, the electromagnetic responses of general natural materials to THz waves are always very weak and cannot meet the requirements for real-world applications. Currently, people put much effort into incremental THz-wave efficiency by using metamaterials [12–14] to enhance the coupling effect between the THz wave and the metamaterial.

Metamaterials are special materials with artificial micro/nanostructures. By adjusting their geometric dimensions, they have many unique electromagnetic responses, including asymmetric transmission, negative refraction index, perfect absorption, and superlens [15–19], and they can work in visible, infrared (IR), THz and microwave spectra ranges [20–23]. Such a unique electromagnetic response can be used in THz optics applications. To date, there has been a significant amount of literature reporting on tunable metamaterials [24,25] by using a split-ring resonator (SRR) [26,27], complementary SRR (CSRR) [28], electric SRR (eSRR) [29], F-shaped SRR [30], V-shaped SRR [31], I-shaped SRR [32], U-shaped SRR [33], C-shaped SRR [34], and three-dimensional SRR [35], etc. However, the tuning ranges of these proposed THz metamaterials are not large enough for the THz filter application. Therefore, the requirement of realizing a tunable THz filter with a large tuning range has become a hot topic of scientific research.

In this study, we propose a tunable THz metamaterial using an eSRR to exhibit polarization-sensitive characteristics. An eSRR is composed of double symmetrical semicircles and two central metal bars on silicon on an insulator (SOI) substrate. By changing the relevant geometrical dimensions of the semicircles and two central metal bars, the resonances of the eSRR device are always stable in transverse electric (TE) mode, and the resonances of TM polarized mode can be tuned with a tuning range of 0.50 THz by moving the bottom metal bar. Moreover, the resonances can be switched between dual-band and triple-band resonances by changing the lengths of two metal bars.

2. Materials and Methods

Figure 1 shows schematic drawings of the 3D view of the eSRR device and the corresponding geometrical denotations of the unit cell. The eSRR device is composed of double symmetrical semicircles and two central metal bars on the SOI substrate. The thickness of the Au layer is kept constant at 300 nm. The corresponding geometrical denotations of the eSRR unit cell are represented in Figure 1b. They are lengths (L_1, L_2) of the metal bars, the gap (g) between the two metal bars, gaps (g_1) between semicircles and bars, and outer and inner radiuses (R, r) of semicircles. The metal line width is kept as a constant at 4 μm. The period of the eSRR is 80 μm × 80 μm. The proposed eSRR device is designed based on finite difference time domain (FDTD) solutions. The periodic boundary conditions are applied along the *x*- and *y*-axis directions, while the boundary condition of the *z*-axis direction is a perfectly matched layer (PML). The monitor of resonant frequency is set under the eSRR device to calculate the transmission of the incident THz wave. The resonant frequency (f_{LC}) can be expressed by [36]:

$$f_{LC} = \frac{1}{2\pi \sqrt{L_{eq}C_{eq}}} = \left(\frac{c_0}{l \sqrt{\varepsilon_c}}\right)\sqrt{\frac{g_{eq}}{w}} \tag{1}$$

where c_0 is the light velocity in a vacuum, L_{eq} and C_{eq} are the equivalent inductance and capacitance of eSRR, ε_c is the relative permittivity of the materials within the eSRR, l is the size of models, w is the metallic line width, and g_{eq} is the equivalent gap width of the eSRR. The resonant frequency of the eSRR can be tuned by changing different parameters. According to Equation (1), the impact of metallic thickness is minor [37–39]. Here, the Au layer is designed to be 300 nm in thickness.
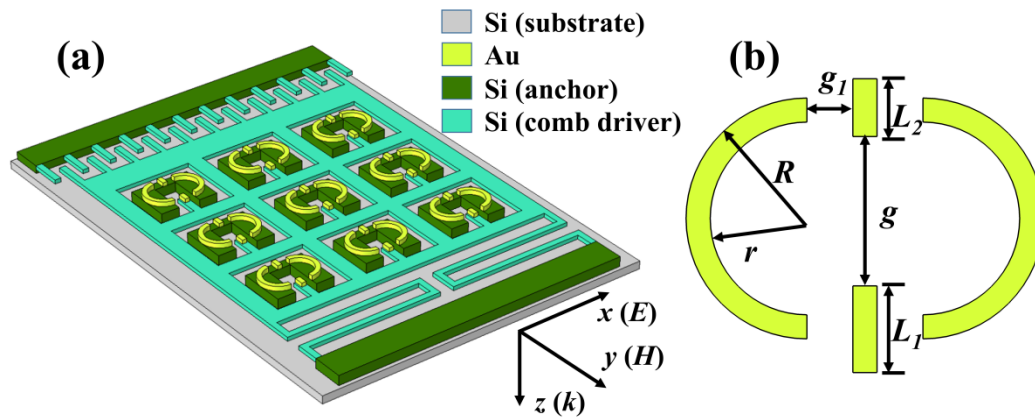

Figure 1. Schematic drawings of (**a**) 3D view of an electric split-ring resonator (eSRR) array and (**b**) geometrical denotations of an eSRR unit cell.

3. Results and Discussion

In our design, the TE electric field is perpendicular to the g_1 parameter, and the transverse magnetic (TM) electric field is perpendicular to the g parameter. To clarify the electromagnetic responses of the eSRR device, we first simulate the transmission spectra of only two metal bars or two semicircles to figure out the source of the individual resonance. Figure 2a,b show the transmission spectra of

metal bars with different L_1 values in TE and TM modes, respectively. By increasing the L_1 value of the bottom metal bar from 12 µm to 24 µm under the condition of $L_2 = 12$ µm, there is no resonance in TE mode and the electromagnetic responses can be switched between dual-band and triple-band resonances in TM mode, as shown in Figure 2a,b, respectively. By increasing the gap between two semicircle-shaped metamaterials (g_0) from 6 to 10 µm under the condition of $R = 20$ µm, there are two stable resonances in TE mode and one stable resonance in TM mode, as shown in Figure 2c,d, respectively. Therefore, we investigate the electromagnetic responses of the eSRR device with different L_1 values by keeping the parameters of $g_1 = 6$ µm, $L_2 = 12$ µm, and $R = 20$ µm, as shown in Figure 3. In TE mode, there are two stable resonances (ω_1, ω_2) at 0.69 and 1.21 THz, as shown in Figure 3a. Meanwhile, by increasing L_1 values, the electromagnetic responses can be tuned and switched between dual-band ($L_1 = L_2$) and triple-band ($L_1 \neq L_2$) resonances in TM mode, as shown in Figure 3b. The first (ω_1) and second (ω_2) resonances are both stable at 0.39 and 1.34 THz, while the third (ω_3) resonance is gradually red-shifted from 1.71 to 0.83 THz by increasing the L_1 value from 8 to 24 µm. The tendencies of resonances and L_1 values of the eSRR device are summarized in Figure 3c. The corresponding electric (E) and magnetic (H) field distributions with $L_1 = 24$ µm are illustrated in Figure 4. In TE mode, the E- and H-field energies are distributed around the semicircles at 0.69 (ω_1) and 1.21 THz (ω_2). In the TM mode, the E- and H-field energies are distributed around the semicircles at 0.39 THz (ω_1). Such a result shows that the first resonance of the eSRR comes from the semicircle structures. The E-field energy is distributed on the upper and lower parts of the upper metal bar, and the H-field energy is distributed in the center of the upper metal bar monitored at 1.34 THz (ω_2). This means that the second resonance of the eSRR is caused by the upper bar. When $f = 0.83$ THz (ω_3), the E-field energy is distributed on the upper and lower parts of the lower metal bar, and the H-field energy is distributed in the center of the lower metal bar, which indicates that the third resonance of the eSRR is generated by the lower bar. Therefore, when the length of the lower bar changes (different L_1 values), the electromagnetic responses of the eSRR can be tuned and switched between the dual-band and triple-band resonances in TM mode.
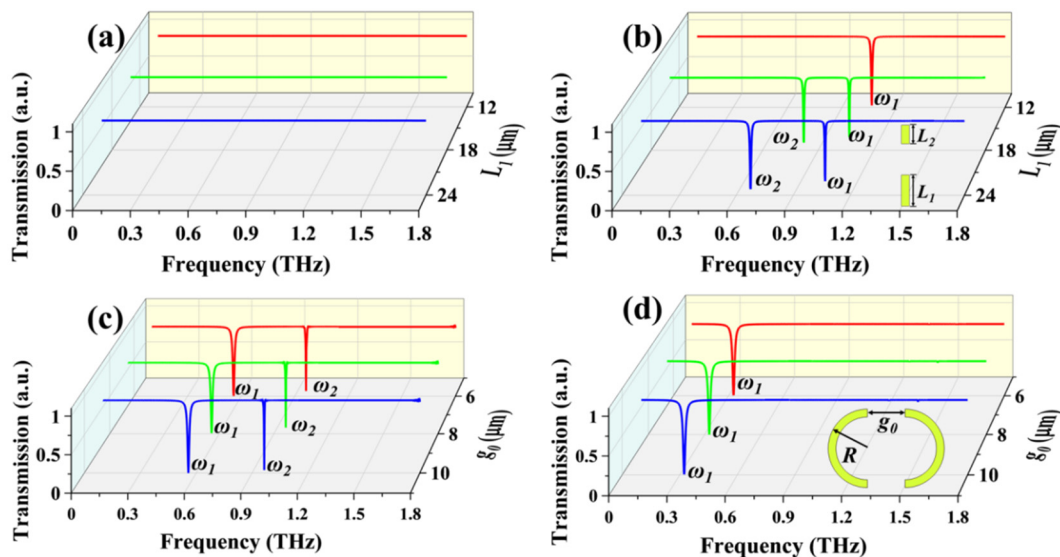
Figure 2. Transmission spectra of metal bars with different L_1 values in (**a**) TE mode and (**b**) transverse magnetic TM mode and those of semicircle-shaped metamaterial with different g_0 values in (**c**) TE mode and (**d**) TM mode, respectively.
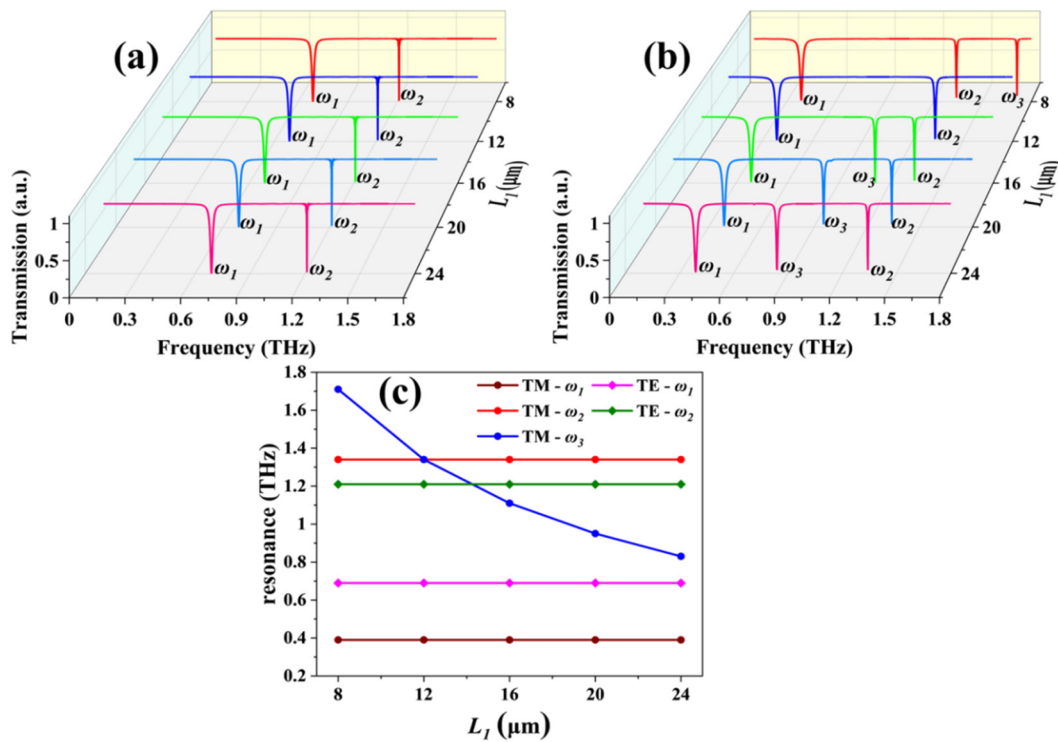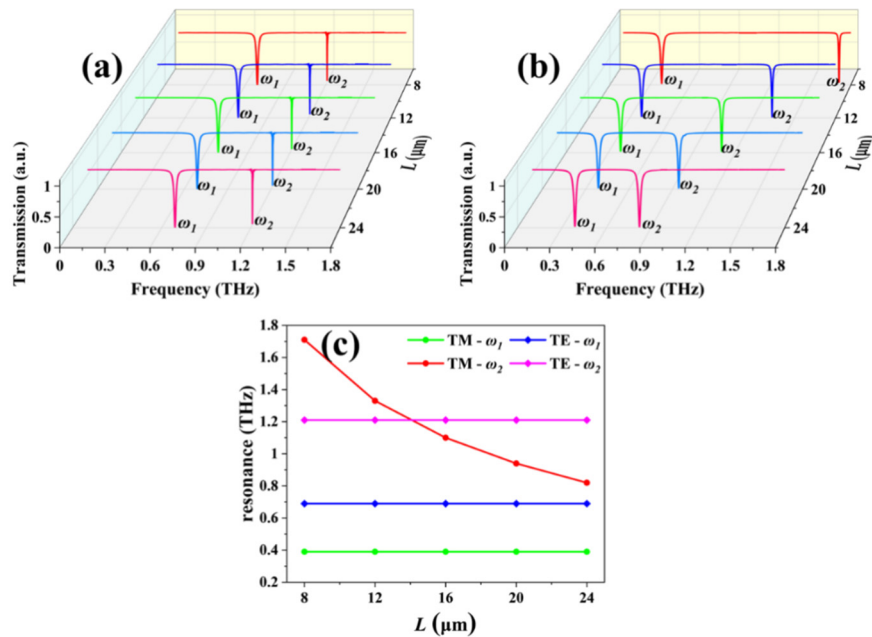
Figure 3. Transmission spectra of eSRR with different L_1 values in (**a**) TE and (**b**) TM modes. (**c**) The relationships between resonances and L_1 values are shown in (**a**,**b**).
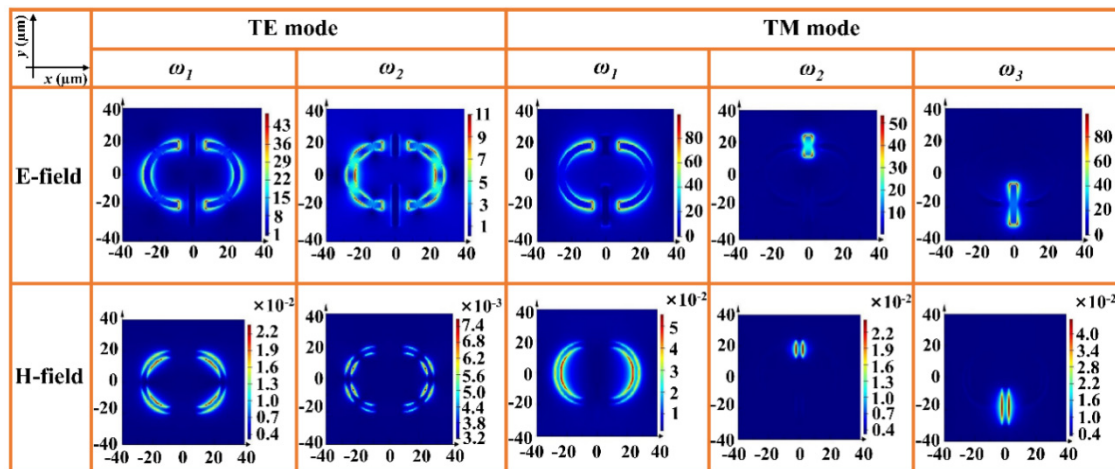
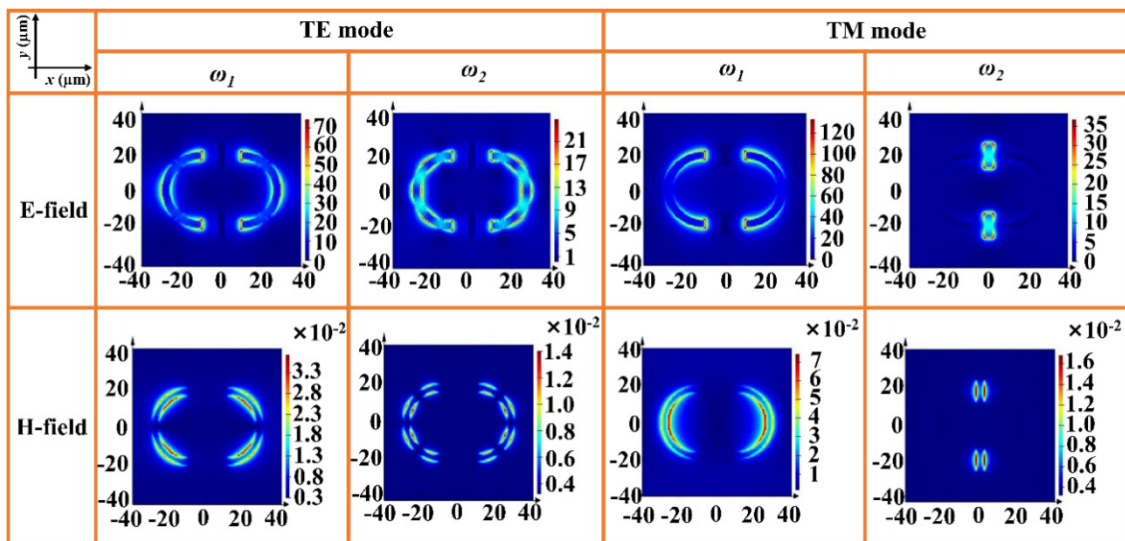**Figure 4.** E- and H-field distributions of eSRR with $L_1 = 24$ μm in TE and TM modes.

When two metal bars are equal at a certain length (i.e., $L = L_1 = L_2$ by keeping $R = 20$ μm and $g_1 = 6$ μm), the corresponding electromagnetic responses of the eSRR device are shown in Figure 5. There are two stable resonances (ω_1, ω_2) at 0.69 and 1.21 THz in TE mode, as shown in Figure 5a. In TM mode, the first resonance (ω_1) is very stable at 0.39 THz, while the second resonance (ω_2) is gradually red-shifted from 1.71 to 0.82 THz by increasing the L value from 8 to 24 μm, as shown in Figure 5b. The tuning range of the second resonance and the free spectrum range (FSR) is 0.89 THz. This characteristic is very suitable for THz filter and sensor applications. The tendency of resonances and L values of the eSRR device are summarized in Figure 5c. Figure 6 represents the corresponding E- and H-field distributions with $L = 12$ μm. It is worth mentioning that the E-field energy is distributed on the upper and lower parts of the two metal bars and the H-field energy is distributed in the center

of the two metal bars monitored at 1.33 THz in TM mode, which is obviously different from the case where the lengths of two metal bars are not equal ($L_1 \neq L_2$).

Figure 5. Transmission spectra of eSRR with different L ($L = L_1 = L_2$) values in (**a**) TE and (**b**) TM modes. (**c**) The relationships of resonances and L values in (**a**,**b**).
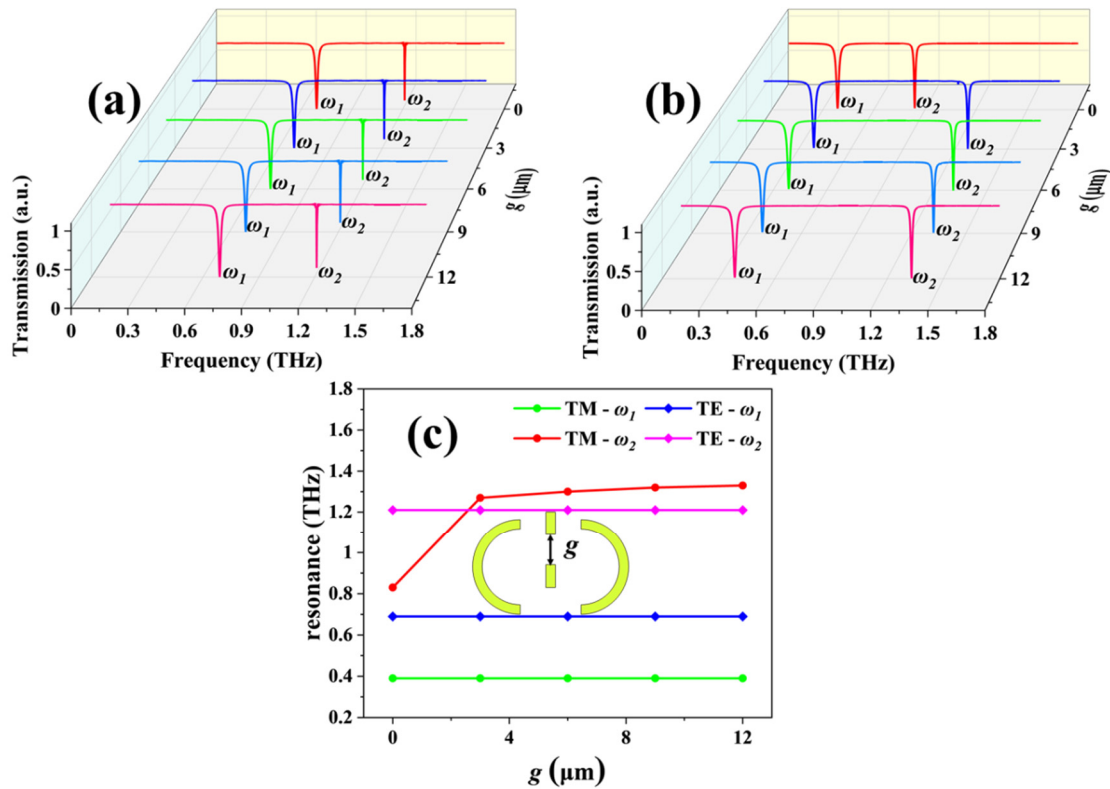

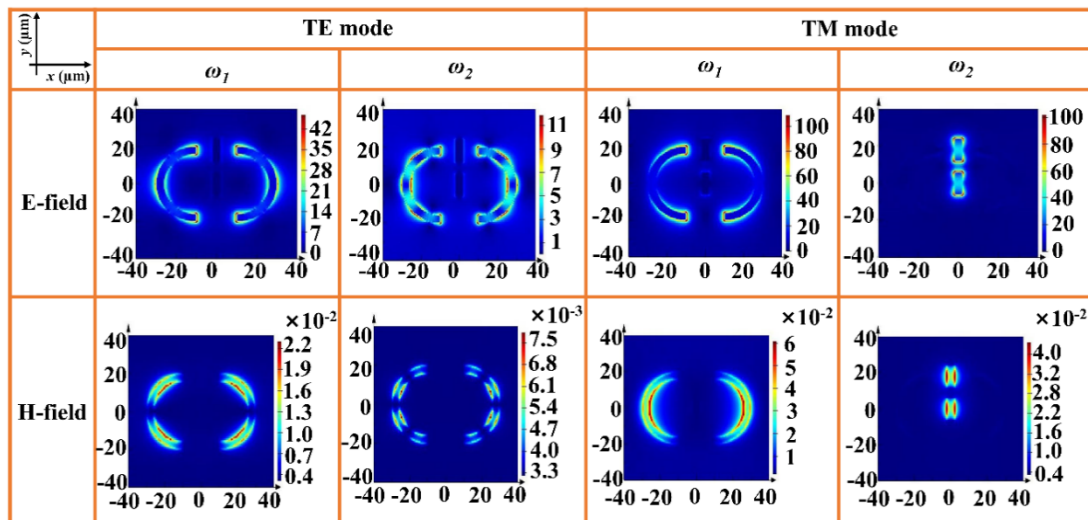**Figure 6.** E- and H-field distributions of eSRR with $L = 12$ μm in TE and TM modes.

The lower metal bar is connected to the suspending microelectromechanical systems (MEMS) comb driver moving along the y-axis direction to change the gap between two metal bars (i.e., g value) and determine tunability and applicability. The transmission spectra of the eSRR with different g values are shown in Figure 7. There are two stable resonances in TE mode, as shown in Figure 7a. In TM mode, the first resonance (ω_1) is very stable at 0.39 THz and the second resonance (ω_2) is gradually blue-shifted from 0.83 to 1.33 THz by increasing the g value from 0 to 12 μm, as shown in Figure 7b. The tuning range is 0.50 THz. That means that FSR can be broadened by 0.50 THz. Therefore, the eSRR could be controlled to broaden the tuning of FSR by increasing the g value and narrowed by increasing the L value, which can be used in a tunable bandwidth filter. The tendencies of resonances and g

values of the eSRR device are summarized in Figure 7c. In order to further understand the physical mechanism of electromagnetic responses of the eSRR, the corresponding E- and H-field distributions of the eSRR with $g = 6$ μm are plotted in Figure 8. The E-field energy is distributed on the upper and lower parts of the two metal bars, and the H-field energy is distributed in the center of the two metal bars monitored at 1.30 THz in TM mode. Therefore, by moving the lower metal bar to a different position, the eSRR device exhibits different optical characteristics. This design provides an effective approach to realize the tunable THz filter, polarizer and sensor applications.

Figure 7. Transmission spectra of an eSRR with different g values in (**a**) TE and (**b**) TM modes. (**c**) The relationships of resonances and g values in (**a**,**b**).

Figure 8. E- and H-field distributions of eSRR with $g = 6$ μm in TE and TM modes.

4. Conclusions

In conclusion, a tunable THz metamaterial using eSRR is presented to demonstrate the electromagnetic responses could be tuned by changing geometrical parameters. By changing the length of the lower metal bar, the electromagnetic responses can be tuned and switched between dual-band and triple-band resonances. The tuning ranges of the FSR can be broadened by 0.50 THz and narrowed by 0.89 THz by changing g and L values, respectively. The eSRR device exhibits tunable and switchable polarization-sensitive characteristics. The gap between semicircles and central metal bars would not influence the electromagnetic response of the eSRR, which indicates that the eSRR device has high stability to allow manufacturing tolerance. These results pave the way for the use of eSRR devices in tunable filters, switches, detectors, sensors and other THz optoelectronics applications.

Author Contributions: Conceptualization, T.X. and Y.-S.L.; methodology, T.X. and Y.-S.L.; software, T.X.; validation, T.X. and Y.-S.L.; formal analysis, T.X. and Y.-S.L.; investigation, T.X. and Y.-S.L.; resources, T.X. and Y.-S.L.; data curation, T.X. and Y.-S.L.; writing—original draft preparation, T.X. and Y.-S.L.; writing—review and editing, T.X. and Y.-S.L.; visualization, T.X. and Y.-S.L.; supervision, Y.-S.L.; project administration, Y.-S.L.; funding acquisition, Y.-S.L. All authors have read and agreed to the published version of the manuscript.

References

1. Booske, J.H.; Dobbs, R.J.; Joye, C.D.; Kory, C.L.; Neil, G.R.; Park, G.-S.; Park, J.; Temkin, R.J. Vacuum Electronic High Power Terahertz Sources. *IEEE Trans. Terahertz Sci. Technol.* **2011**, *1*, 54–75. [CrossRef]
2. Shi, W.; Ding, Y.J.; Fernelius, N.; Vodopyanov, K.L. An efficient tunable and coherent 0.18–5.27 terahertz source based on GaSe crystal. *Opt. Lett.* **2002**, *27*, 1454–1456. [CrossRef] [PubMed]
3. Libon, I.H.; Hecker, N.E.; Koch, M.; Baumgartner, S.; Hempel, M.; Feldmann, J.; Dawson, P. An optically controllable terahertz filter. *Appl. Phys. Lett.* **2000**, *76*, 2821–2823. [CrossRef]
4. Wu, X.; Quan, B.; Pan, X.; Xu, X.; Lu, X.; Gu, C.-Z.; Wang, L. Alkanethiol-functionalized terahertz metamaterial as label-free, highly-sensitive and specificbiosensor. *Biosens. Bioelectron.* **2013**, *42*, 626–631. [CrossRef] [PubMed]
5. Ahi, K. Mathematical Modeling of THz Point Spread Function and Simulation of THz Imaging Systems. *IEEE Trans. Terahertz Sci. Technol.* **2017**, *7*, 747–754. [CrossRef]
6. Petrov, N.; Kulya, M.; Tsypkin, A.N.; Bespalov, V.G.; Gorodetsky, A. Application of Terahertz Pulse Time-Domain Holography for Phase Imaging. *IEEE Trans. Terahertz Sci. Technol.* **2016**, *6*, 464–472. [CrossRef]
7. Van Der Weide, D.; Murakowski, J.; Keilmann, F. Gas-absorption spectroscopy with electronic terahertz techniques. *IEEE Trans. Microw. Theory Tech.* **2000**, *48*, 740–743. [CrossRef]
8. Yan, X.; Yang, M.; Zhang, Z.; Liang, L.; Wei, D.; Wang, M.; Zhang, Z.; Wang, T.; Liu, L.; Xie, J.; et al. The terahertz electromagnetically induced transparency-like metamaterials for sensitive biosensors in the detection of cancer cells. *Biosens. Bioelectron.* **2019**, *126*, 485–492. [CrossRef]
9. Lannebère, S.; Campione, S.; Aradian, A.; Albani, M.; Capolino, F. Artificial magnetism at terahertz frequencies from three-dimensional lattices of TiO_2 microspheres accounting for spatial dispersion and magnetoelectric coupling. *J. Opt. Soc. Am. B* **2014**, *31*, 1078. [CrossRef]
10. Fan, Y.; Zhang, F.; Zhao, Q.; Wei, Z.; Li, H. Tunable terahertz coherent perfect absorption in a monolayer graphene. *Opt. Lett.* **2014**, *39*, 6269–6272. [CrossRef]
11. Ou, H.; Lu, F.; Xu, Z.; Lin, Y.-S. Terahertz Metamaterial with Multiple Resonances for Biosensing Application. *Nanomaterials* **2020**, *10*, 1038. [CrossRef] [PubMed]
12. Zheng, D.; Hu, X.; Lin, Y.-S.; Chen, C.-H. Tunable multi-resonance of terahertz metamaterial using split-disk resonators. *AIP Adv.* **2020**, *10*, 025108. [CrossRef]
13. Lu, F.; Ou, H.; Liao, Y.; Zhu, F.; Lin, Y.-S. Actively switchable terahertz metamaterial. *Results Phys.* **2019**, *15*, 102756. [CrossRef]

14. Xu, Z.; Lin, Z.; Cheng, S.; Lin, Y.-S. Reconfigurable and tunable terahertz wrench-shape metamaterial performing programmable characteristic. *Opt. Lett.* **2019**, *44*, 3944–3947. [CrossRef] [PubMed]

15. Xu, Z.; Lin, Y.-S. A Stretchable Terahertz Parabolic-Shaped Metamaterial. *Adv. Opt. Mater.* **2019**, *7*, 1900379. [CrossRef]

16. Lin, Y.-S.; Liao, S.; Liu, X.; Tong, Y.; Xu, Z.; Xu, R.; Yao, D.; Yu, Y. Tunable terahertz metamaterial by using three-dimensional double split-ring resonators. *Opt. Laser Technol.* **2019**, *112*, 215–221. [CrossRef]

17. Liu, P.; Liang, Z.; Lin, Z.; Xu, Z.; Xu, R.; Yao, D.; Lin, Y.-S. Actively tunable terahertz chain-link metamaterial with bidirectional polarization-dependent characteristic. *Sci. Rep.* **2019**, *9*, 9917. [CrossRef]

18. Xu, R.; Liu, X.; Lin, Y.-S. Tunable ultra-narrowband terahertz perfect absorber by using metal-insulator-metal microstructures. *Results Phys.* **2019**, *13*, 102176. [CrossRef]

19. Luo, J.; Lin, Y.-S. High-efficiency of infrared absorption by using composited metamaterial nanotubes. *Appl. Phys. Lett.* **2019**, *114*, 051601. [CrossRef]

20. Zhan, F.; Lin, Y.S. Tunable Multi-Resonance Using Complementary Circular Metamaterial. *Opt. Lett.* **2020**, *45*, 3633–3636. [CrossRef]

21. Lin, Y.-S.; Yan, K.; Yao, D.; Yu, Y. Investigation of electromagnetic response of terahertz metamaterial by using split-disk resonator. *Opt. Laser Technol.* **2019**, *111*, 509–514. [CrossRef]

22. Lin, Y.-S.; Dai, J.; Zeng, Z.; Yang, B.-R. Metasurface Color Filters Using Aluminum and Lithium Niobate Configurations. *Nanoscale Res. Lett.* **2020**, *15*, 77. [CrossRef] [PubMed]

23. Xu, R.; Lin, Y.-S. Characterizations of reconfigurable infrared metamaterial absorbers. *Opt. Lett.* **2018**, *43*, 4783–4786. [CrossRef] [PubMed]

24. Gómez-Castaño, M.; Zheng, H.; Garcia-Pomar, J.L.; Vallée, R.A.L.; Mihi, A.; Ravaine, S. Tunable index metamaterials made by bottom-up approaches. *Nanoscale Adv.* **2019**, *1*, 1070–1076. [CrossRef] [PubMed]

25. Weis, P.; Garcia-Pomar, J.L.; Rahm, M. Towards loss compensated and lasing terahertz metamaterials based on optically pumped graphene. *Opt. Express* **2014**, *22*, 8473–8489. [CrossRef] [PubMed]

26. Pendry, J.; Holden, A.; Robbins, D.; Stewart, W. Magnetism from conductors and enhanced nonlinear phenomena. *IEEE Trans. Microw. Theory Tech.* **1999**, *47*, 2075–2084. [CrossRef]

27. Ma, F.; Lin, Y.-S.; Zhang, X.; Lee, V.C. Tunable multiband terahertz metamaterials using a reconfigurable electric split-ring resonator array. *Light. Sci. Appl.* **2014**, *3*, e171. [CrossRef]

28. Lan, F.; Yang, Z.; Qi, L.; Gao, X.; Shi, Z. Terahertz dual-resonance bandpass filter using bilayer reformative complementary metamaterial structures. *Opt. Lett.* **2014**, *39*, 1709–1712. [CrossRef]

29. Yu, Y.; Lin, Y.-S. Multi-functional terahertz metamaterial using symmetrical and asymmetrical electric split-ring resonator. *Results Phys.* **2019**, *13*, 102321. [CrossRef]

30. Lin, Z.; Xu, Z.; Liu, P.; Liang, Z.; Lin, Y.-S. Polarization-sensitive terahertz resonator using asymmetrical F-shaped metamaterial. *Opt. Laser Technol.* **2020**, *121*, 105826. [CrossRef]

31. Kishor, K.; Baitha, M.N.; Sinha, R.K.; Lahiri, B. Tunable negative refractive index metamaterial from V-shaped SRR structure: Fabrication and characterization. *J. Opt. Soc. Am. B* **2014**, *31*, 1410. [CrossRef]

32. Cao, W.; Zhang, B.; Liu, A.; Yu, T.; Guo, D.; Wei, Y. Broadband High-Gain Periodic Endfire Antenna by Using I-Shaped Resonator (ISR) Structures. *IEEE Antennas Wirel. Propag. Lett.* **2012**, *11*, 1470–1473. [CrossRef]

33. Lin, Y.-S.; Huang, C.-Y.; Lee, V.C. Reconfiguration of Resonance Characteristics for Terahertz U-Shape Metamaterial Using MEMS Mechanism. *IEEE J. Sel. Top. Quantum Electron.* **2014**, *21*, 93–99. [CrossRef]

34. Zhang, Z.; Zhang, X.; Liang, Z.; Cheng, S.; Liu, P.; Lin, Y.-S. Reconfigurable double C-shape metamaterial (DCM) for a terahertz resonator. *OSA Contin.* **2019**, *2*, 3026–3036. [CrossRef]

35. Ma, F.; Qian, Y.; Lin, Y.-S.; Liu, H.; Zhang, X.; Liu, Z.; Tsai, J.M.; Lee, V.C. Polarization-sensitive microelectromechanical systems based tunable terahertz metamaterials using three dimensional electric split-ring resonator arrays. *Appl. Phys. Lett.* **2013**, *102*, 161912. [CrossRef]

36. Mo, Y.; Zhong, J.; Lin, Y.-S. Tunable chevron-shaped infrared metamaterial. *Mater. Lett.* **2020**, *263*, 127291. [CrossRef]

37. Ou, H.; Lu, F.; Liao, Y.; Zhu, F.; Lin, Y.-S. Tunable terahertz metamaterial for high-efficiency switch application. *Results Phys.* **2020**, *16*, 102897. [CrossRef]

38. Cheng, S.; Xu, Z.; Yao, D.; Zhang, X.; Zhang, Z.; Lin, Y.-S. Electromagnetically induced transparency in terahertz complementary spiral-shape metamaterials. *OSA Contin.* **2019**, *2*, 2137–2144. [CrossRef]

39. Hu, X.; Zheng, D.; Lin, Y.-S. Actively tunable terahertz metamaterial with single-band and dual-band switching characteristic. *Appl. Phys. A* **2020**, *126*, 110. [CrossRef]